II-306 Sand-barrier Flushing in Shinguu River Mouth during a Flood

O H.S.Jin, S.Egashira, H.Nakagawa and S.Sekine
Member, Faculty of Sci. & Eng., Ritsumeikan Univ.
1916 Noji, Kusatsu, Shiga 525

1. Introduction Estuarine flows are usually affected very much by the presence of spits. These arise because coastal currents and river flows have supplied a large amount of material. A representative sand barrier is formed at the estuary of Shinguu river. Usually it is almost closed, the flow width of waterway is only about 10% of the river width. The location and scale of the barrier change very actively, mainly depending on magnitudes of waves and floods. Fig.1 shows the sand barrier measured in Feb., 1990. Such a sand-barrier may cause flood hazards because the resulted water surface level rises additionally during floods. However, the waterway gradually expands due to the lateral erosion when the discharge increases and the water surface level rises. Part of the sand barrier is flushed when the flow discharge exceeds a critical condition, which depends on variables such as sediment property, wind waves, tidal motion and so on. The present study discusses the process of water stages and sand barrier flushing which are evaluated in terms of a 2-D mathematical model.

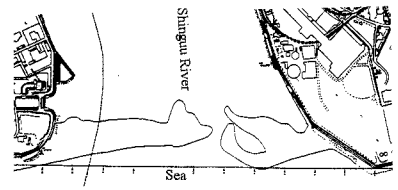

Fig.1 Sand barrier in Shinguu river

2. Description of the method Calculational domain is shown in fig.2 which is about 7km long with two bends. Numerically generated boundary-fitted orthogonal curvilinear coordinate system, as shown in fig.2, is employed due to very irregular boundaries of the domain. Only bedload is considered in the following evaluation of bed-deformation. Governing equations for water flow and bedload transport are expressed below:

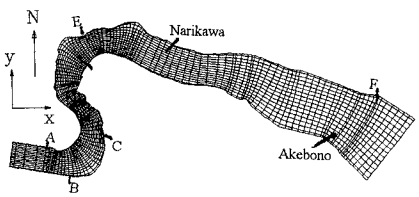

Fig.2 Calculational domain and grid system

$$\frac{\partial h}{\partial t}+\frac{1}{J}\left[\frac{\partial(u^{*}hg_{22})}{\partial\xi}+\frac{\partial(v^{*}hg_{11})}{\partial\eta}\right]=0 \tag{1}$$

$$\frac{\partial u^{*}}{\partial t}+\frac{u^{*}}{g_{11}}\frac{\partial u^{*}}{\partial\xi}+\frac{v^{*}}{g_{22}}\frac{\partial u^{*}}{\partial\eta}+\frac{u^{*}v^{*}}{J}\frac{\partial g_{11}}{\partial\eta}-\frac{v^{*2}}{J}\frac{\partial g_{22}}{\partial\xi}=-\frac{g}{g_{11}}\frac{\partial\zeta}{\partial\xi}+\frac{1}{\rho hJ}\left[\frac{\partial}{\partial\xi}(hg_{22}\sigma_{11})+\frac{\partial}{\partial\eta}(hg_{11}\tau_{12})\right]+\frac{\tau_{21}}{\rho J}\frac{\partial g_{11}}{\partial\eta}-\frac{\sigma_{22}}{\rho J}\frac{\partial g_{22}}{\partial\xi}+\frac{\tau_{s\xi}-\tau_{b\xi}}{\rho h}+fv^{*} \tag{2}$$

$$\frac{\partial v^{*}}{\partial t}+\frac{u^{*}}{g_{11}}\frac{\partial v^{*}}{\partial\xi}+\frac{v^{*}}{g_{22}}\frac{\partial v^{*}}{\partial\eta}+\frac{u^{*}v^{*}}{J}\frac{\partial g_{22}}{\partial\xi}-\frac{u^{*2}}{J}\frac{\partial g_{11}}{\partial\eta}=-\frac{g}{g_{22}}\frac{\partial\zeta}{\partial\eta}+\frac{1}{\rho hJ}\left[\frac{\partial}{\partial\xi}(hg_{22}\tau_{21})+\frac{\partial}{\partial\eta}(hg_{11}\sigma_{22})\right]+\frac{\tau_{12}}{\rho J}\frac{\partial g_{22}}{\partial\xi}-\frac{\sigma_{11}}{\rho J}\frac{\partial g_{11}}{\partial\eta}+\frac{\tau_{s\eta}-\tau_{b\eta}}{\rho h}-fu^{*} \tag{3}$$

$$\frac{\partial Z_{b}}{\partial t}+\frac{1}{1-\lambda}\frac{1}{g_{11}g_{22}}\frac{\partial}{\partial\xi}(g_{22}q_{b\xi})+\frac{\partial}{\partial\eta}(g_{11}q_{b\eta})=0 \tag{4}$$

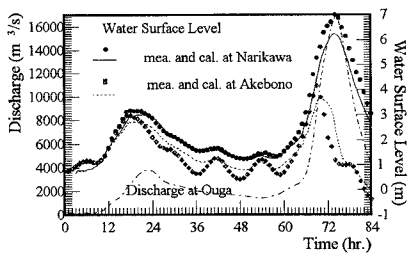

Fig.3 Hydrograph of ζ and discharge

where ξ and η are the orthogonal curvilinear coordinate components; g_{11}, g_{22} and J are the coordinate transformation relationships[1]; u^{*} and v^{*} are the ξ and η component of depth-averaged velocity respectively; ζ, Z_b and h are the water surface level, bed level, and water depth respectively; ρ, g, λ and f are the density of water, gravity acceleration, porosity of bed sediment and Coriolis coefficient respectively. σ_{11}, $\tau_{12}=\tau_{21}$ and σ_{22} are the depth-averaged effective stress; τ_s and τ_b are the shear stress at the water surface and stream bed, respectively[1]. q_b is the volumetric bedload transport rate and is evaluated with Ashida-Michiue's formula[2]. In addition, the direction of bedload movement is determined by flow velocity near bed in terms of curvature of streamline and incline of local bed[3].

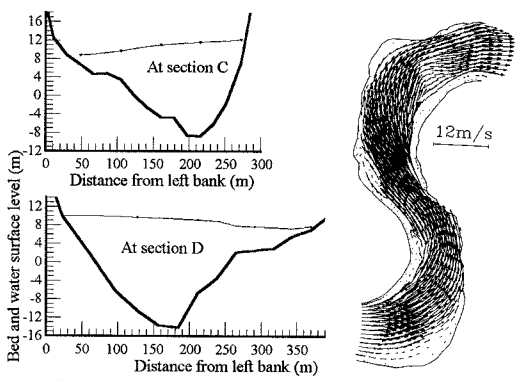

(a) Water surface super-elevation (b) Flow field
Fig.4 Water surface and flow field in bends

Eqs.(1)~(3) are discretized by finite difference scheme and solved by TDMA with ADI method[1] first, and then streamline and velocity near bed are calculated. Finally bed level is evaluated with eq.(4). A grid "block" technique is introduced to overcome the computational difficulty caused by the unsteady fluctuation of water surface level.[1]

3. Boundary and initial conditions At the downstream boundary, real-time tidal elevation is employed. Temporal flow-rate is specified at the upstream boundary. The impenetrable condition is applied to the bank boundaries, i.e., the velocity normal to the bank is equal to zero and the tangent one is not zero. Equilibrium bedload transport is assumed at the open boundaries. The initial conditions are specified according to the corresponding boundary value at starting time.

Based on sampling analysis, mean diameter—14.9mm is chosen for the reference diameter of bedload. Flood discharge course measured at Ouga during 17~20 Sept. 1990 is taken as the inflow condition.

4. Result and analysis Comparison of calculated water surface levels with measured data at Narikawa and Akebono is displayed in fig.3. Water surface super-elevation and flow field in bend reach between section B and D are demonstrated in fig.4. These show that the present method reproduces the change of water surface level and the water surface super-elevation and velocity redistribution in bend very well. Fig.5 shows the longitudinal profiles of water surface level and bed elevation at deepest point. Velocity vector around sand barrier is designated in fig.6. The barrier is submerged gradually with increase of flood discharge. The water surface slope around the barrier is very steep and the flow pattern is complicated before it is flushed. Fig.7 and 8 show the bed elevation contour around the barrier and the cross section variation on the barrier, respectively. These results demonstrate that the barrier is eroded only a little during the previous small flood, however, it is flushed due to the succeeding main flood. During the main flood, sand barrier is eroded gradually and is flushed for 4~5hrs. before the peak.

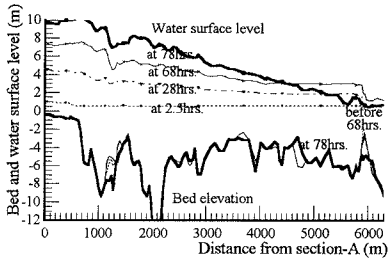

Fig.5 Longitudinal profile at deepest point

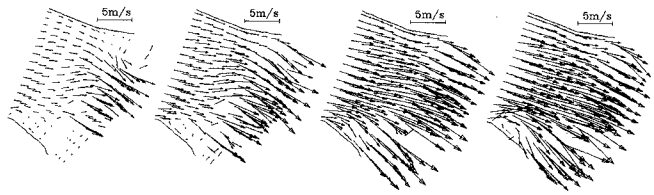

(a)at 66hrs. (b)at 69hrs. (c)at 72hrs. (d)at 74hrs.

Fig.6 Velocity vector around the sand barrier

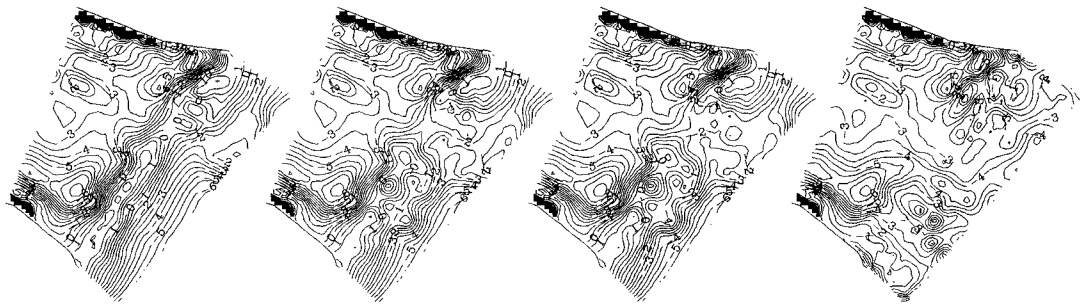

(a)at 2.5hrs. (b)at 28hrs. (c)at 68hrs. (d)at 78hrs.

Fig.7 Bed elevation contour at different time

5. Conclusions From the above results, it can be concluded that the present method is preferable for describing the flushing process of sand barrier in Shinguu river due to flood event.

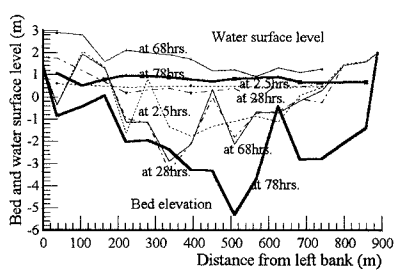

Fig.8 Bed variation at section F

6. References

(1) Jin,H.S., S.Egashira, Y.M.Zheng and G.B.Yuan (1996), Numerical simulation of flow in 'T'-shaped tidal river, Proceeding of the 3rd APCOM, Seoul, Korea.

(2) Ashida,K., S.Egashira and Y.Adachi (1988), Study on the bed variation in a meandering channel, The annuals of the DPRI, Kyoto Univ., 31(B-2).

(3) Liu,B.Y.(1991), Study on sediment transport and bed evolution in compound channels. Doct.diss., Kyoto Univ.